Available online at www.sciencedirect.com
ScienceDirect
Ceramics International 38 (2012) 159–168
CERAMICS INTERNATIONAL
www.elsevier.com/locate/ceramint

Oxidation behavior and kinetics of in situ $(TiB_2 + TiC)/Ti_3SiC_2$ composites in air

J. Yang *, L.M. Pan, W. Gu, X.B. Gu, K. Song, T. Qiu, S.M. Zhu

College of Materials Science and Engineering, Nanjing University of Technology, Nanjing 210009, China

Received 23 October 2010; received in revised form 3 January 2011; accepted 4 May 2011
Available online 1st July 2011

Abstract

The isothermal oxidation behavior of in situ $(TiB_2 + TiC)/Ti_3SiC_2$ composite ceramics with different TiB_2 content has been investigated at 900–1200 °C in air for exposure times up to 20 h by means of X-ray diffraction, Fourier transform infrared spectroscopy, scanning electron microscopy, and energy dispersive spectroscopy. The oxidation of $(TiB_2 + TiC)/Ti_3SiC_2$ composites follows a parabolic rate law. With the increase in TiB_2 content, the oxidation weight gain, thickness of the oxidation scale, and parabolic rate constant decrease dramatically, which suggests that the incorporation of TiB_2 greatly improves the oxidation resistance of the composites. With the increase in oxidation temperature, the enhancement effect becomes more pronounced. Due to the incorporation of TiB_2, the oxidation scale of $(TiB_2 + TiC)/Ti_3SiC_2$ composites is generally composed of an outer layer of coarse-grained TiO_2 and an inner layer of amorphous boron silicate and fine-grained TiO_2. Only the dense inner layer formed on the surface acts as a diffusion barrier, retarding the inward diffusion of O, and consequently contributing to the improved oxidation resistance of the $(TiB_2 + TiC)/Ti_3SiC_2$ composites.

Keywords: $(TiB_2 + TiC)/Ti_3SiC_2$ composite; TiB_2; Oxidation resistance; Mechanism

1. Introduction

Ti_3SiC_2 is a representative ternary-layered carbide that combines the merits of metals and ceramics, such as low density, high modulus, good thermal and electrical conductivity, excellent thermal shock resistance and high-temperature strength, damage tolerance, and easy machinability [1–5]. Therefore, it is a promising candidate for new high-temperature structural materials, electrode material in molten metals, self-lubricating material, and electric brush material. However, low hardness, creep strength, oxidation and wear resistance of Ti_3SiC_2 restrict potential application. Incorporation of second phase is an effective way to overcome these weaknesses. A number of reinforcing agents, including TiC, SiC, Al_2O_3, c-BN, TiB_2, and ZrO_2, have been applied to improve the mechanical properties of Ti_3SiC_2 [6–11]. However, previous studies mainly concentrated on composites containing only one reinforcing agent and limited enhancement effect. As a structural ceramic for high-temperature applications, the ability to resist oxidation is the primary criterion apart from adequate strength and good creep resistance. Therefore, the oxidation behavior of Ti_3SiC_2 and Ti_3SiC_2-based materials has been investigated by a number of researchers [12–16]. Sun et al. [14] reported that the TiC content in Ti_3SiC_2 was deleterious to its oxidation resistance, although TiC/Ti_3SiC_2 composites show enhanced mechanical properties compared with monolithic Ti_3SiC_2.

Both TiB_2 and TiC are ideal candidate reinforcements for Ti_3SiC_2 matrix in view of their high hardness, high modulus, excellent chemical stability, good electrical and thermal conductivity, and approximate coefficient of thermal expansion with Ti_3SiC_2. Compared with the traditional preparation process, in situ synthesis shows many advantages in fabrication of composite ceramics, such as uniform distribution and fine grain size of the reinforcements, clean and tightly bonded grain boundaries, simplified process, and excellent properties. In our previous study, $(TiB_2 + TiC)/Ti_3SiC_2$ composites have been successfully prepared by in situ hot-pressing sintering, in which the Ti_3SiC_2 matrix is synergistically reinforced by columnar TiB_2 and equiaxed TiC grains. Due to the synergistic action of the strengthening and toughening mechanisms, such as

* Corresponding author. Tel.: +86 25 83587262; fax: +86 25 83587268.
E-mail address: yangjian1976@163.com (J. Yang).

0272-8842/$36.00 © 2011 Published by Elsevier Ltd and Techna Group S.r.l.
doi:10.1016/j.ceramint.2011.05.156

particulate reinforcement, crack deflection, grain pull-out, and fine-grain toughening caused by the two reinforcing agents, the composites show excellent mechanical properties [17]. In $(TiB_2 + TiC)/Ti_3SiC_2$ composites, the oxidation of elements B and Si may be expected to result in a dense borosilicate protective film formed on the surface of the composites and to produce intelligent self-healing oxidation resistance effect.

In the present study, isothermal oxidation resistance of the as-prepared $(TiB_2 + TiC)/Ti_3SiC_2$ composites in the temperature range of 900–1200 °C up to 20 h was investigated, and the effect of TiB_2 content on the oxidation behavior of the composites was determined. Related mechanisms were attentively discussed.

2. Experimental procedure

TiH_2 (99.9%, 300 mesh), Si (99.9%, 300 mesh), graphite (99.9%, 200 mesh), and B_4C (99%, average particle size 3.5 μm) were used to prepare in situ $(TiB_2 + TiC)/Ti_3SiC_2$ composites according to the general reaction as follows:

$$(3 + 3x + y)TiH_2 + Si + (2 + y)C + xB_4C \rightarrow TiSiC_2 + 2xTiB_2 + (x + y)TiC + (3 + 3x + y)H_2\uparrow \quad (1)$$

The composites (the volume fraction of TiC in the composites was fixed at 10 vol.%) with different TiB_2 content were denoted as TC (0 vol.%), TC/5B (5 vol.%), TC/10B (10 vol.%), TC/15B (15 vol.%) and TC/20B (20 vol.%), respectively. Excess Si (1.2 mol Si) was added to ensure that the obtained TiC volume content in $(TiB_2 + TiC)/Ti_3SiC_2$ composites was close to the theoretical one. After being mixed and dried, the mixtures were heated at 900 °C for 1 h and then hot pressed at 1500 °C for 2 h under an Ar atmosphere at 25 MPa.

To determine the true phase composition in the $(TiB_2 + TiC)/Ti_3SiC_2$ composites, quantitative phase analysis was conducted using X-ray diffraction (XRD) by the Rietveld method [18]. The XRD data were collected by a step-scanning diffractometer with Cu Kα radiation (Rigaku D/max 2500/PC, Japan) at 40 kV and 200 mA. The data used for quantitative analysis had accuracy better than 0.02°. Table 1 compares the target TiB_2 contents with those determined from quantitative phase analysis using the Rietveld method. It is clear that the theoretical contents of TiB_2 and TiC are quite close to the calculated ones. Thus, we adopt the target TiB_2 volume content to represent each sample in the following part. The apparent porosity of the samples is also listed in Table 1. It can be seen that all the samples show a high density (apparent porosity is lower than 0.15%), which suggests that the effect of density or pores for oxidation behavior can be ignored in the present study.

For the oxidation experiments, rectangular bars with the dimensions of 10 mm × 3 mm × 4 mm were cut via the electrical-discharge method. The surfaces were ground down with 1000 SiC paper and polished using diamond paste. Subsequently, the samples were ultrasonically cleaned in acetone to remove the paste residue. The oxidation test was performed in a high-temperature furnace at a temperature range of 900–1200 °C for exposures up to 20 h. The weight gain was calculated by the difference after and before the oxidation tests using an electric balance with an accuracy of 1×10^{-7} kg. After the oxidation tests, the samples were characterized by X-ray diffraction to determine the phase composition of the oxide scale. The composition and chemical bonding structures of the inner layer were also determined using Fourier transform infrared (FT-IR) spectroscopy. The surface, cross-sectional, and inner layer morphologies of the oxidized samples were observed by a scanning electron microscope (SEM) equipped with energy dispersive spectroscopy (EDS).

Table 1
The target contents of TiB_2 and TiC compared with those calculated by the Rietveld method in $(TiB_2 + TiC)/Ti_3SiC_2$ composites. The apparent porosity of the samples is also listed.

Sample	The target contents (vol.%)		The calculated contents by the Rietveld method (vol.%)		Apparent porosity (%)
	TiB_2	TiC	TiB_2	TiC	
TC	0	10	0	9.7	0.147
TC/5B	5	10	5.2	10.3	0.045
TC/10B	10	10	8.8	11.6	0.124
TC/15B	15	10	14.1	11.4	0.128
TC/20B	20	10	18.9	14.3	0.042

3. Results and discussion

3.1. Oxidation kinetics

Fig. 1 shows the weight gain per unit area as a function of time for the composites at different temperatures. At 900–1200 °C, the weight gain per unit area decreases with the increase in TiB_2 content of the composites, which is clearer at high temperatures. The weight gain of TC at 1200 °C for 20 h was 71.99×10^{-2} kg m^{-2}, whereas that of TC/20B was only 22.92×10^{-2} kg m^{-2}, which is about 30% of the former. The results suggest that the in situ incorporation of TiB_2 improves the oxidation resistance of the composites, which is more significant with increasing TiB_2 content and oxidation temperature. The corresponding square of weight gain per unit area as a function of time at 1100 and 1200 °C is shown in Fig. 2. The oxidation behavior of $(TiB_2 + TiC)/Ti_3SiC_2$ composites (0–20 vol.% TiB_2) was found to follow the

Table 2
A summary of parabolic rate constant and activation energy for all the samples.

Sample	Parabolic rate constant ($k \times 10^{-6}$)				Activation energy (kJ mol^{-1})
	900 °C	1000 °C	1100 °C	1200 °C	
TC	0.015	0.75	2.85	7.64	293
TC/5B	0.011	0.37	0.97	1.53	234
TC/10B	0.011	0.32	0.71	0.89	209
TC/15B	0.007	0.28	0.69	0.80	222
TC/20B	0.006	0.21	0.63	0.73	228

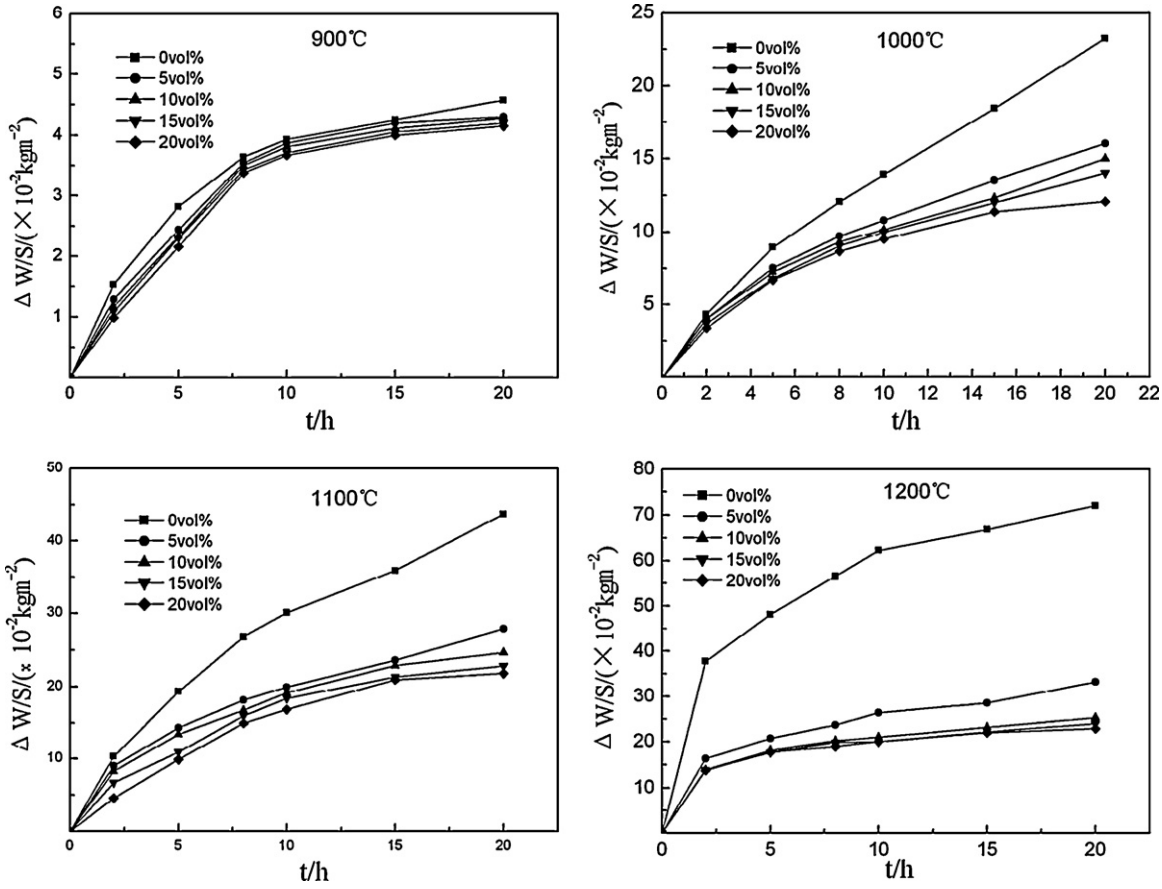

Fig. 1. Weight gain per unit area versus time oxidized at 900–1200 °C for the composites with different TiB_2 content.

parabolic rule. However, the oxidation kinetics of sample TC follows a two-step parabolic oxidation process, i.e., the first stage from 0 to 9 h and the second stage from 10 to 20 h. The parabolic rate constant decreases at the second stage of oxidation, which suggests the formation of a protective scale or layer that inhibits further oxidation. Table 2 shows the parabolic rate constants for all the samples oxidized at different temperatures. The table shows that the parabolic rate constant also decreases greatly because of the incorporation of TiB_2 particles. The parabolic rate constant of TC/20B oxidized at 1200 °C was 0.73×10^{-6} kg^2 m^{-4} s^{-1}, which is an order of magnitude lower than that of the TiC/Ti_3SiC_2 composite. Therefore, (TiB_2 + TiC)/Ti_3SiC_2 composites generally possess better resistance to oxidation than TiC/Ti_3SiC_2.

Table 2 also gives the activation energy for the oxidation process from 900 to 1200 °C, which was obtained from the temperature dependence of the parabolic rate constants. It can be seen that the activation energy for TC is 293 kJ mol^{-1}, which is in agreement with the result of Barsoum et al. [12], 300 ± 15 kJ mol^{-1}, in the temperature of 900–1200 °C. Note that (TiB_2 + TiC)/Ti_3SiC_2 composites exhibit lower activation energy as well as oxidation rate than TiC/Ti_3SiC_2 composite

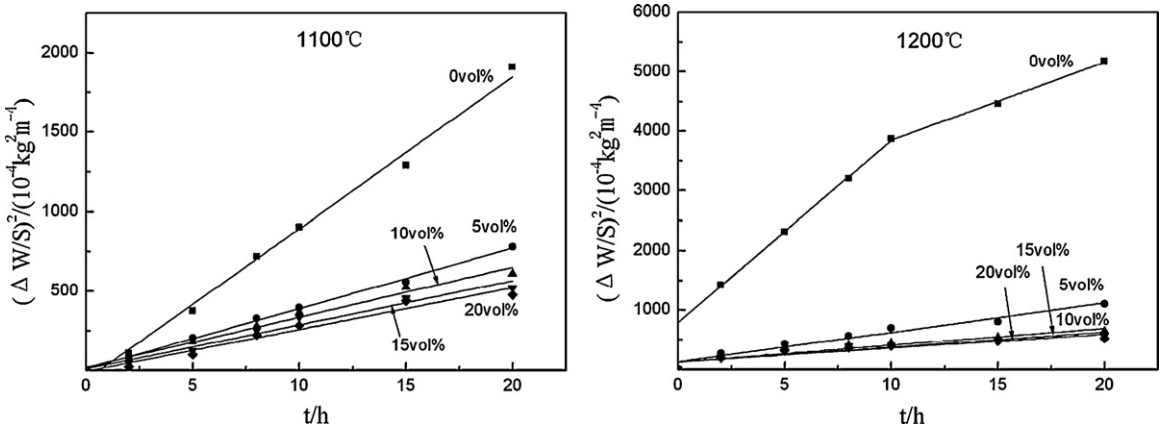

Fig. 2. Square of weight gain per unit area versus time for the composites with different TiB_2 content oxidized at 1100 and 1200 °C.

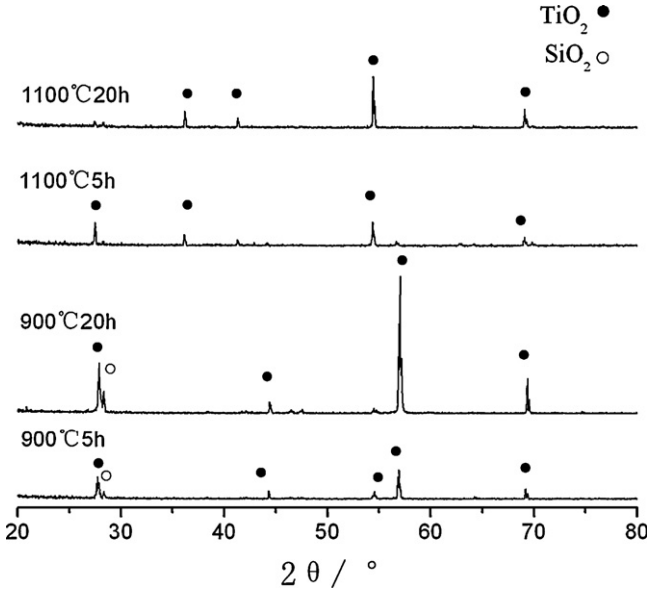

Fig. 3. XRD patterns of the oxide surfaces on the TC sample oxidized at different temperatures for different time.

(TC). The discrepancy here is not clear at present and it is under further investigation.

3.2. Phase composition of oxide scales

Figs. 3 and 4 show the XRD patterns of the surface of the TC and TC/20B samples oxidized at 900 and 1100 °C, respectively. TiO_2 with small amounts of SiO_2 can be detected from XRD results after oxidation of TC and TC/20B at 900 °C up to 20 h. The presence of SiO_2 is due to the very thin layer of the oxide scale. When the temperature rose to 1100 °C, different evolution of oxidation products occurred in the two composites. For TC, nearly no SiO_2 peak could be detected and the oxidized surface was only composed of TiO_2 (rutile) even after exposure to air for 5 h. However, for TC/20B, a small amount of SiO_2 was detected in the oxidation surface at 5 h, which was not identified as oxidation time was prolonged to 20 h. This indicates that the thickness of the oxide scale increases with oxidation temperature and time. On the other hand, TC/20B has a thinner oxide scale than TC. In addition, the TiO_2 peaks became sharper with the increase in oxidation temperature and prolongation of oxidation time, which implies enhanced growth and development of TiO_2 grains.

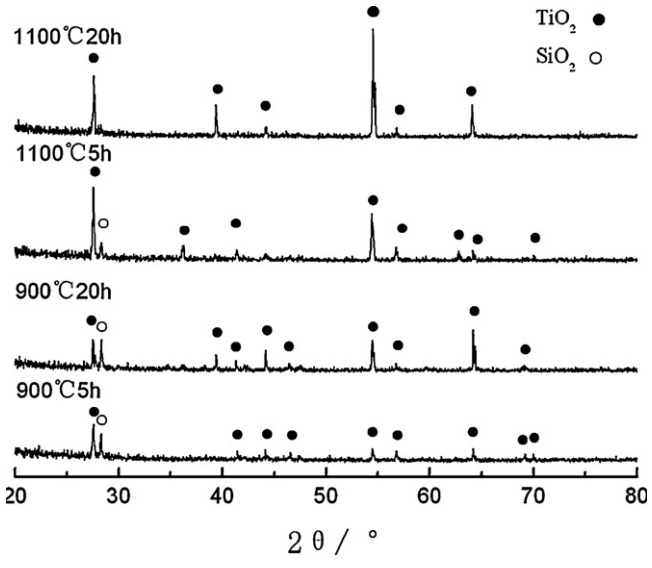

Fig. 4. XRD patterns of the oxide surfaces on the TC/20B sample oxidized at different temperatures for different time.

3.3. Morphology evolution of oxide scales

3.3.1. Surface morphology

Figs. 5 and 6 show the surface morphology and EDS spectra of the TC and TC/20B samples oxidized at 900 and 1100 °C, respectively. TC and TC/20B show similar surface morphology evolution with oxidation temperature and time. Well-shaped crystals were formed on the oxidized surfaces. EDS analysis indicates that these crystals contain mainly Ti and O. Small amount of Si was also detected, which gradually disappeared with increasing oxidation temperature and time. EDS results are in good agreement with the former XRD results, which suggests that the oxidized surfaces are covered mainly by TiO_2 grains. The crystal size increases greatly with increasing oxidation temperature and time. However, TC/20B possesses smaller grain sizes in the oxidized surface compared with TC under the same oxidation conditions, which may be attributed to the fact that the former has a finer-grained microstructure compared with the latter due to the inhibitory effect of TiB_2 incorporation on the grain growth of the Ti_3SiC_2 matrix.

3.3.2. Phase compositions and morphologies of sectioned samples

Figs. 7 and 8 show the typical cross-sectional morphology and EDS microanalysis of the TC and TC/20B samples oxidized at 900 and 1100 °C, respectively. As shown in the figures, the oxidation scale of TC and TC/20B consists of two distinct parts. The coarse-grained bright layers on the left of the micrographs were identified as TiO_2, whereas the dark gray layers in the middle of the micrographs contain Ti, Si, and O. The parts on the right are the matrix. Therefore, the oxidation scale generally consists of an outer part of coarse-grained TiO_2 and an inner part of a fine-grained microstructure containing Ti, Si, and O. The TiO_2 in the outer layer grows very quickly without any restraint and develops into the coarse grains. However, the grain growth in the inner layer is prevented by the outer layer, which results in the finer grain formation. The above feature is similar to that reported by Zhang et al. [14,16]. However, in the present investigation, there were no cracks observed at the interface between oxidation scale and matrix, suggesting good adhesion between the oxidation scale and the substrate. As determined in Figs. 7 and 8, after oxidation at 900 and 1100 °C for 20 h, the oxidation scale thickness of TC/20B was approximately 70 and 210 μm, respectively, which are much lower than that of TC (230 and 750 μm). The incorporation of TiB_2 significantly reduces the thickness of

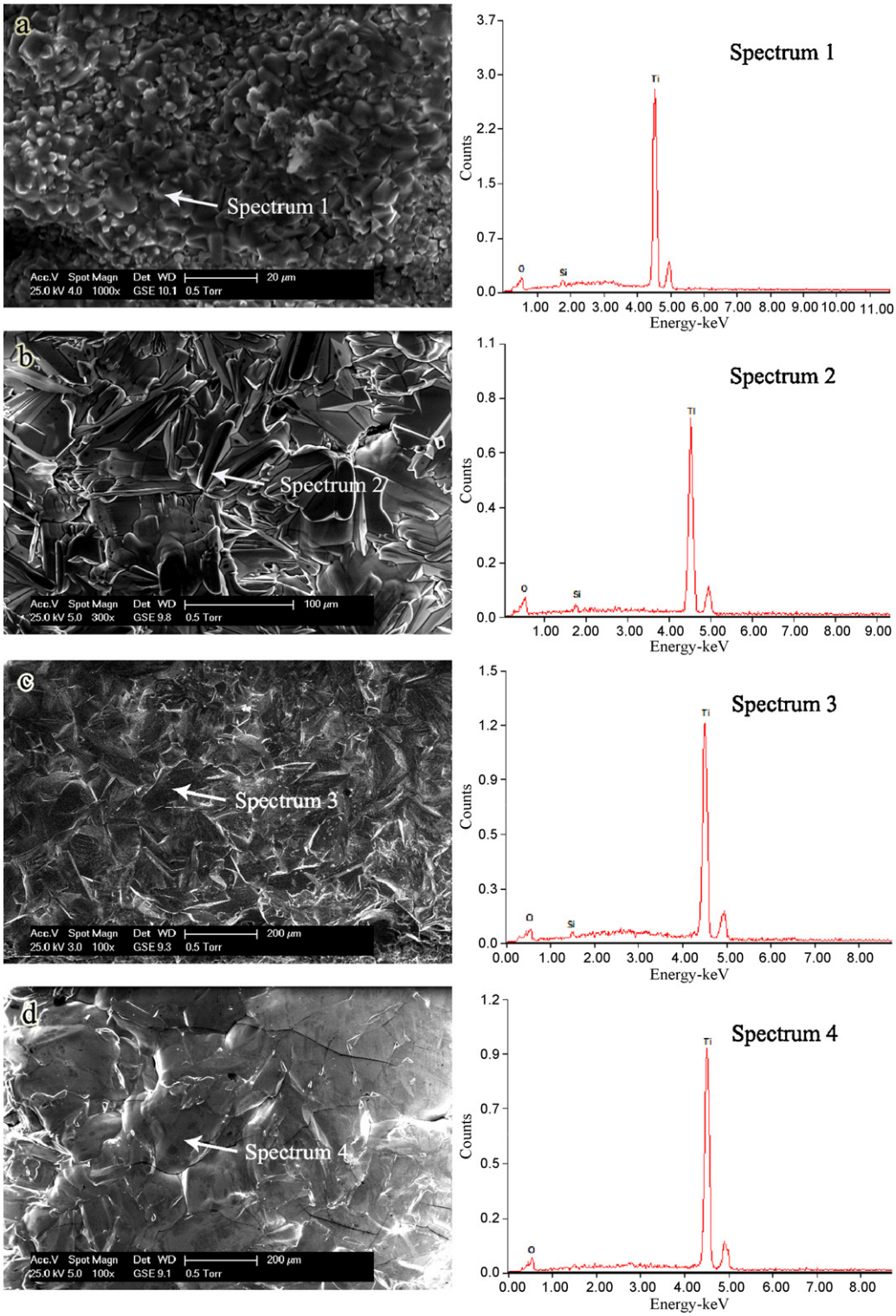

Fig. 5. Surface morphology and EDS spectra of oxide scales for the sample TC: 900 °C, 5 h; (b) 900 °C, 20 h; (c) 1100 °C, 5 h; and (d) 1100 °C, 20 h.

oxidation scale, retards the oxidation, and improves the oxidation resistance of the composites.

Fig. 9 shows the XRD pattern of the inner layer of TC/20B oxidized at 1100 °C for 15 h, in which five sharp peaks and one broad peak were detected. The five sharp peaks were determined as TiO_2 (rutile), whereas the broad peak represents an amorphous substance existing in the inner layer. To reveal further the composition and structure of the amorphous substance, the FT-IR spectroscopy was applied and the result is shown in Fig. 10. Three distinct absorption peaks at approximately 1023.3, 1371.9, and 916.8 cm^{-1} are shown. The peak at 1023.3 cm^{-1} can be interpreted as the asymmetrical

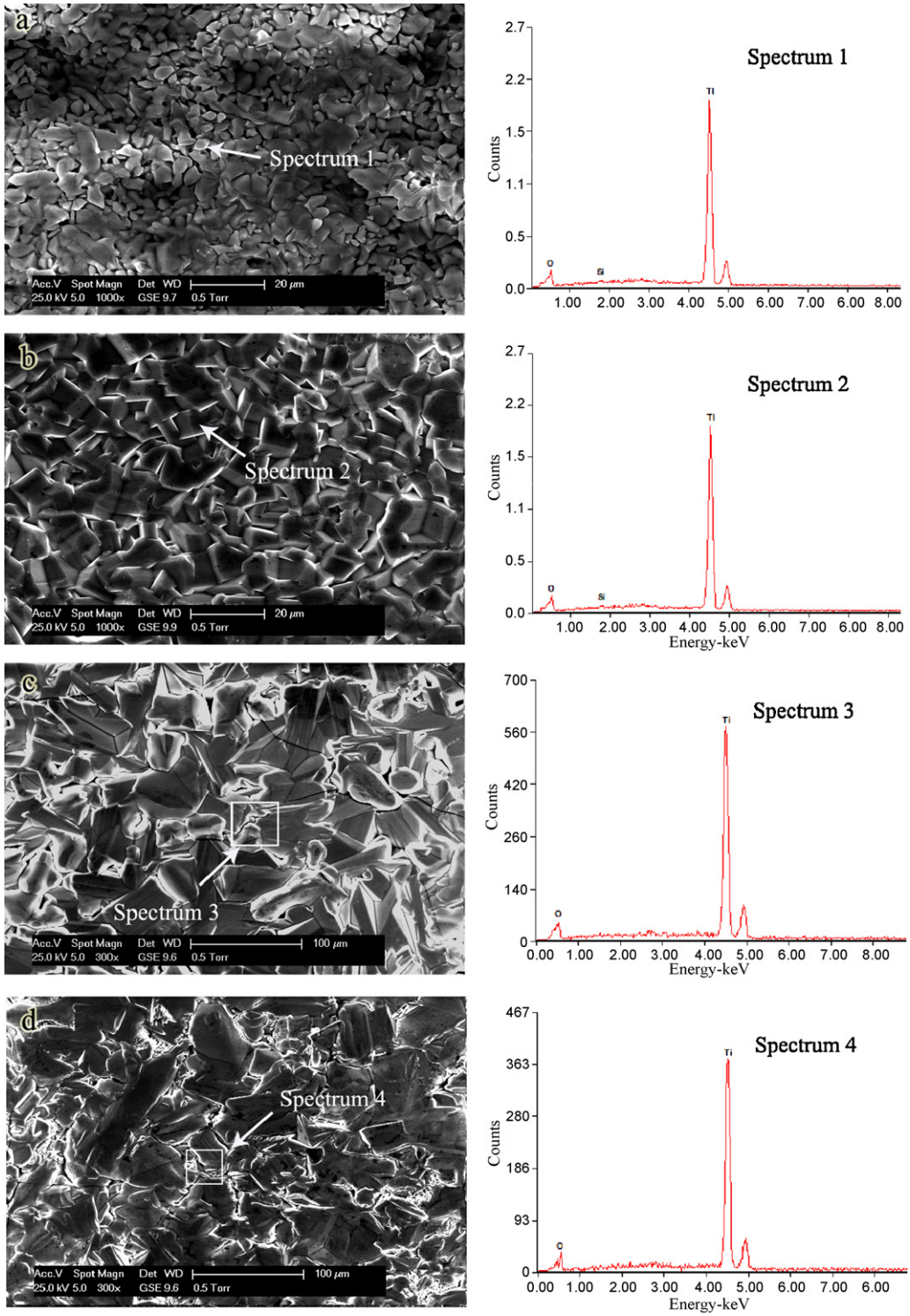

Fig. 6. Surface morphology and EDS spectra of oxide scales for the sample TC/20B: (a) 900 °C, 5 h; (b) 900 °C, 20 h; (c) 1100 °C, 5 h; and (d) 1100 °C, 20 h.

stretching vibration of tetrahedral $B_{(4)}$–O bond [19]. The peak at 1371.9 cm^{-1} represents the vibration of the B–O–Si bond [20]. The absorption at 916.8 cm^{-1} is widely accepted as the vibration of the Si–O bond. According to the FT-IR analysis, it seems that the amorphous substance in the inner layer of the oxidized (TiB_2 + TiC)/Ti_3SiC_2 was boron silicate.

Figs. 11 and 12 show the morphology and EDS spectra of the inner layer for the TC and TC/20B oxidized at 1100 °C for 15 h, respectively. For the TC composite, a loose inner layer with many interconnected interstices composed of crystallites and amorphous substances was observed. Those interstices provide the channels for oxygen diffusion and accelerate the oxidation process. Those crystallites marked "1" and the amorphous areas marked "2" were identified as TiO_2 and SiO_2 by EDS, respectively. This feature is in accordance with the results reported for TiC/Ti_3SiC_2 composites by other researchers [15].

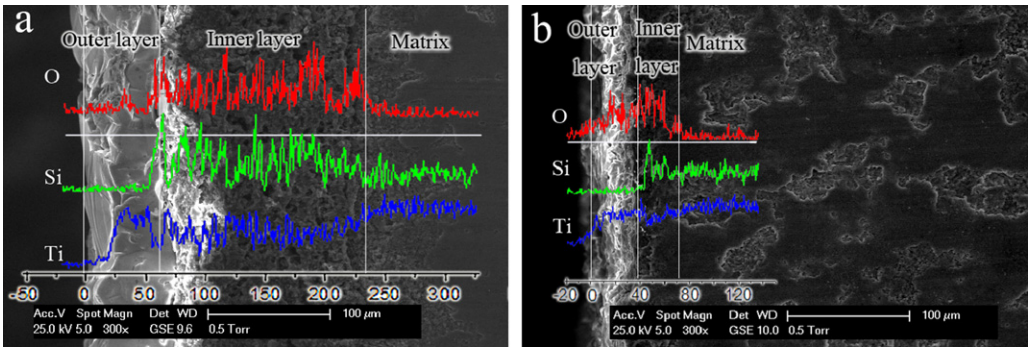

Fig. 7. SEM micrographs and EDS elemental distribution of cross section of the oxide scales of the composites after exposure to air for 20 h at 900 °C: (a) sample TC; (b) sample TC/20B.

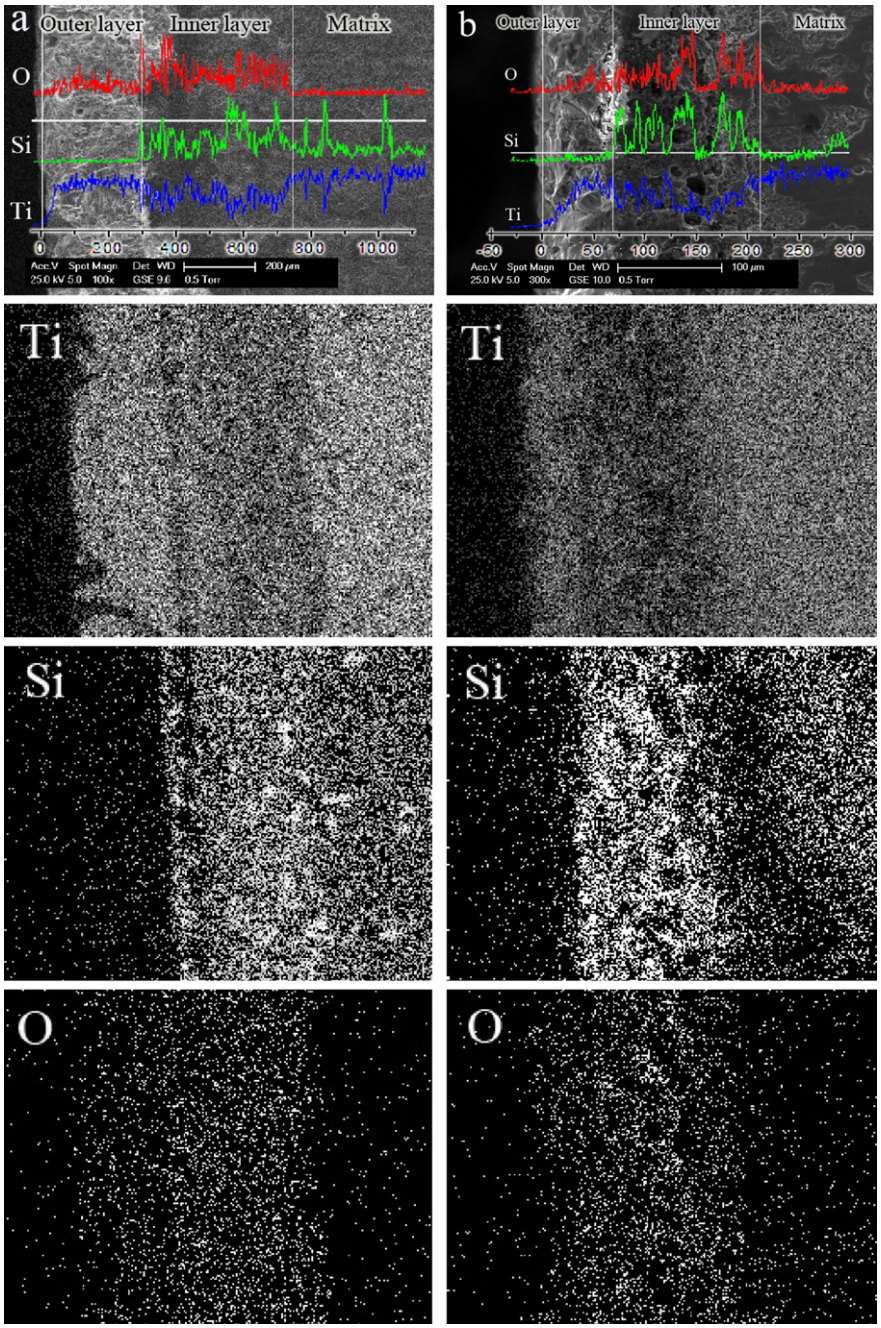

Fig. 8. SEM micrographs and EDS elemental distribution of cross section of the oxide scales of the composites after exposure to air for 20 h at 1100 °C: (a) sample TC; (b) sample TC/20B.

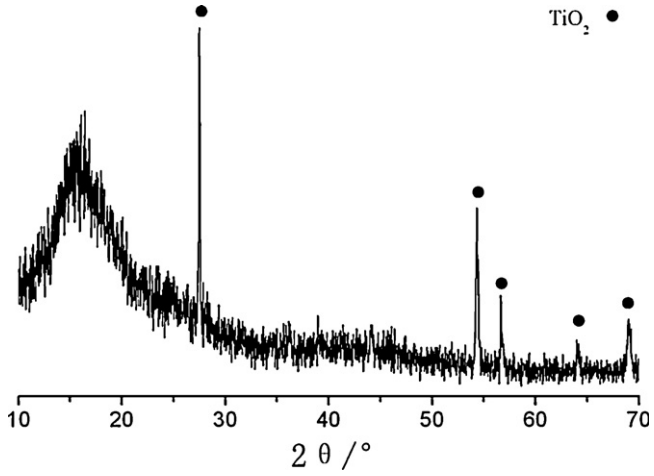

Fig. 9. XRD pattern of the oxide inner layer on the sample TC/20B oxidized at 1100 °C for 15 h.

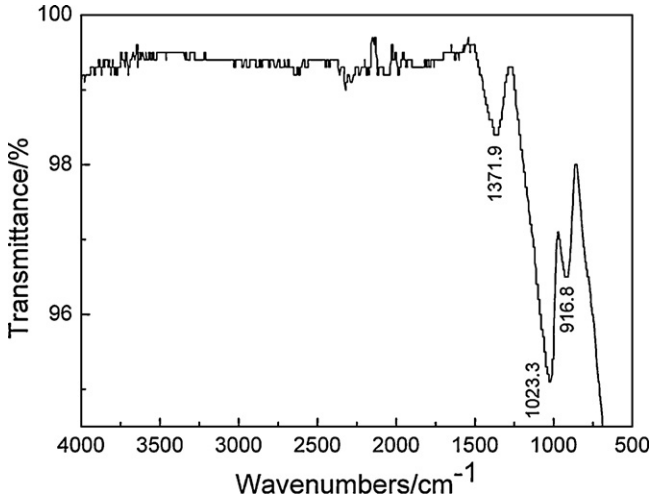

Fig. 10. FT-IR spectrum of the oxide inner layer on the sample TC/20B oxidized at 1100 °C for 15 h.

In contrast, in TC/20B, the inner layer consists of a great amount of dense amorphous substances with some isolated small pores and no obvious crystallites could be observed. However, in consideration of the EDS spectrum (as shown in Fig. 12) and the former XRD result, the fine TiO_2 grains are presumably encapsulated or covered by the amorphous substances.

In conclusion, the inner layer of the $(TiB_2 + TiC)/Ti_3SiC_2$ composites consists of small TiO_2 grains and amorphous boron silicate.

3.4. Oxidation mechanism

Previous works by Barsoum et al. [21] and Sun et al. [14] proposed that the oxidation of Ti_3SiC_2 is a diffusion-controlled process, i.e., the process is controlled by the inward diffusion of oxygen and outward diffusion of titanium and carbon, and the Si sublattice was essentially immobile. The outer TiO_2 layer grew by outward diffusion of Ti, whereas the inner layer of the fine-grained mixture of TiO_2

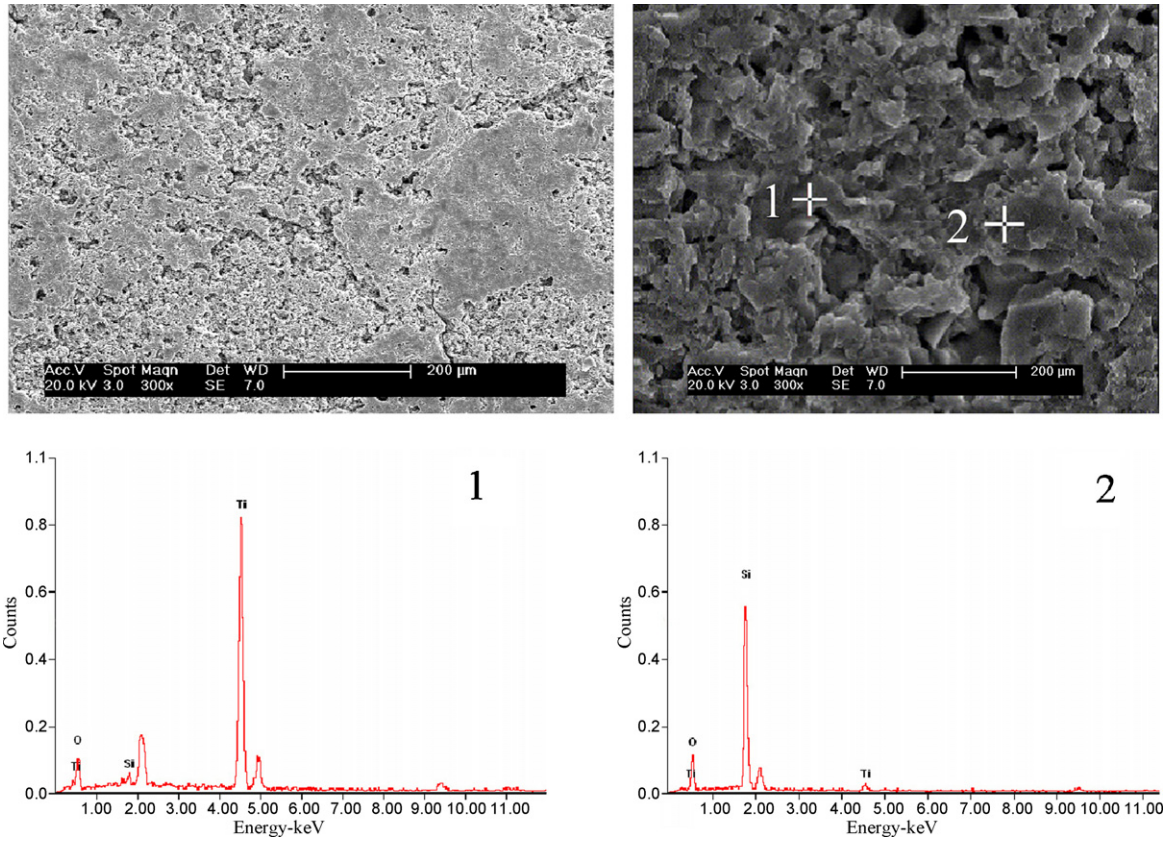

Fig. 11. Surface morphologies and EDS spectra of the inner layer of the oxide scale for the TC sample oxidized at 1100 °C for 15 h.

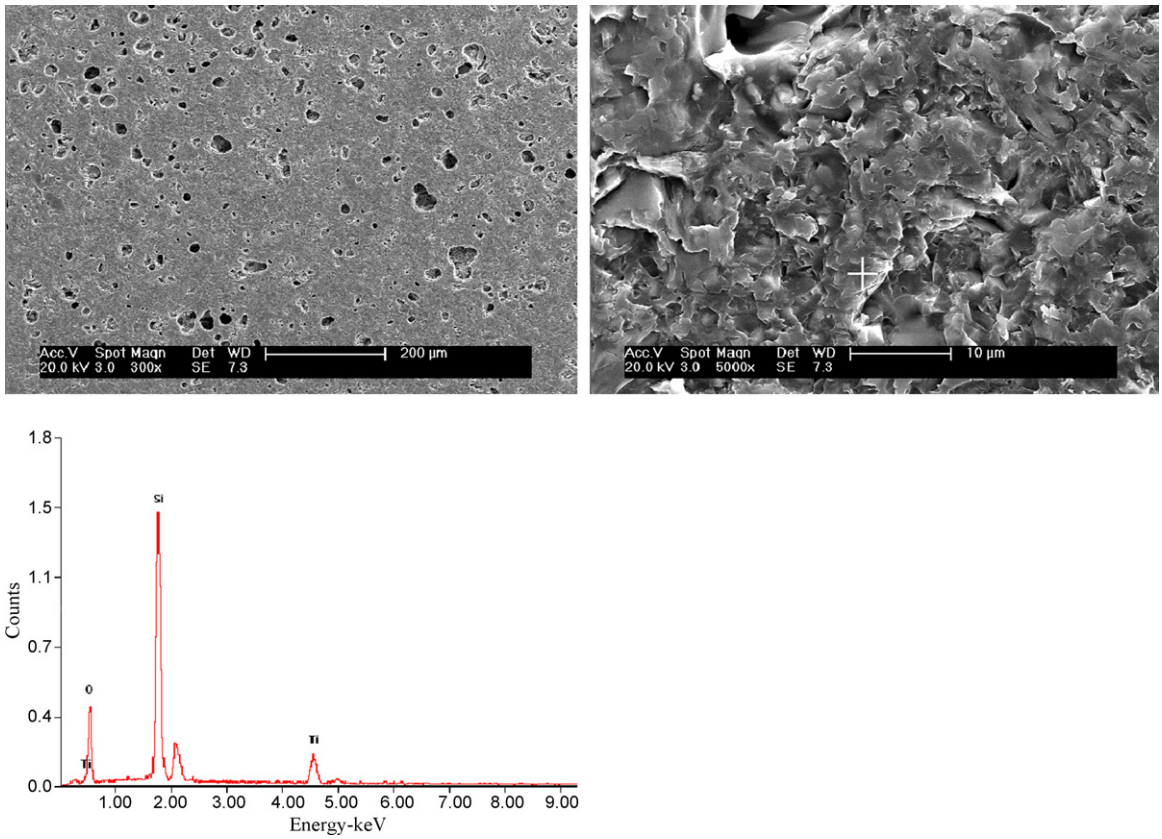

Fig. 12. Surface morphologies and EDS spectra of the inner layer of the oxide scale for the TC/20B sample oxidized at 1100 °C for 15 h.

and SiO_2 grew by the inward diffusion of oxygen. The total reaction is as follows:

$$Ti_3SiC_2 + 5O_2(g) \rightarrow 3TiO_2 + SiO_2 + 2CO(g) \quad (2)$$

TiO_2 cannot protect the matrix from oxidation because TiO_2 would grow to be loose and coarse grained in the outer layer. Only the inner layer composed of fine TiO_2 and SiO_2 would retard the diffusion and protect the matrix from oxidation.

For the oxidation of $(TiB_2 + TiC)/Ti_3SiC_2$ composites, the above analysis has demonstrated that the transport of Ti, Si, C, and O in the scale followed the same rule. The oxidation scale also consists of two layers and the outer layer is mainly composed of large TiO_2 grains. However, the incorporation of TiB_2 provides the $(TiB_2 + TiC)/Ti_3SiC_2$ composites with some unique oxidation mechanisms different from those of Ti_3SiC_2 and other Ti_3SiC_2-matrix composites. During the oxidation of $(TiB_2 + TiC)/Ti_3SiC_2$ composites, TiB_2 and TiC will be oxidized first

$$TiC + 2O_2(g) \rightarrow TiO_2 + CO_2(g) \quad (3)$$

$$TiB_2 + \tfrac{5}{2}O_2 \rightarrow TiO_2 + B_2O_3 \quad (4)$$

The oxidation product B_2O_3 further reacts with SiO_2, producing a large amount of amorphous boron silicate. For $(TiB_2 + TiC)/Ti_3SiC_2$ composites, amorphous boron silicate and fine-grained TiO_2 constitute a dense oxidation film that acts as a diffusion barrier, retarding the diffusion of oxygen and the further oxidation of the materials, which accounts for the excellent oxidation resistance of the composites. The presence of small pores in the inner layer may have resulted from the volatilization of B_2O_3, which has a low melting point of 450 °C, during the oxidation process.

4. Conclusions

The oxidation dynamics of $(TiB_2 + TiC)/Ti_3SiC_2$ composites at 900–1200 °C in air follows the parabolic law. With the increase in TiB_2 content, the oxidation weight gain, thickness of oxidation scale, and parabolic rate constant decreased dramatically, which suggests that the incorporation of TiB_2 greatly improves the oxidation resistance of the composites. With the increase in oxidation temperature, the enhancement effect becomes more pronounced. The parabolic rate constant of the $(TiB_2 + TiC)/Ti_3SiC_2$ composite with 20 vol.% TiB_2 oxidized at 1200 °C was 0.73×10^{-6} kg^2 m^{-4} s^{-1}, which is an order of magnitude lower than that of the TiC/Ti_3SiC_2 composite.

During oxidation, TiB_2, TiC, and Ti_3SiC_2 are oxidized, which produces an oxidation scale generally composed of an outer layer of coarse-grained TiO_2 and an inner layer of amorphous boron silicate and fine-grained TiO_2. Only the dense inner layer formed on the surface acts as a diffusion barrier, retarding the inward diffusion of O, and consequently contributing to the improved oxidation resistance of $(TiB_2 + TiC)/Ti_3SiC_2$ composites.

Acknowledgements

This work was supported by the National Natural Science Foundation of China under Grant No. 50872052, National High Technology Research and Development Program ('863' project) under Grant No. 2009AA05Z313, Natural Science Foundation of Jiangsu Province Education Commission under Grant No. 07KJB430039, and the Key Laboratory of New Inorganic Materials and its Composites, Jiangsu Province.

References

[1] M.W. Barsoum, The $M_{N+1}AX_N$ phases: a new class of solids; thermodynamically stable nanolaminates, Prog. Solid State Chem. 28 (1–4) (2000) 201–281.
[2] V.D. Jovic, B.M. Jovic, S. Gupta, et al., Corrosion behavior of select MAX phases in NaOH, HCl and H_2SO_4, Corros. Sci. 48 (12) (2006) 4274–4282.
[3] M. Radovic, M.W. Barsoum, A. Ganguly, et al., On the elastic properties and mechanical damping of Ti_3SiC_2, Ti_3GeC_2, $Ti_3Si_{0.5}Al_{0.5}C_2$ and Ti_2AlC in the 300–1573 K temperature range, Acta Mater. 54 (10) (2006) 2757–2767.
[4] H.I. Yoo, M.W. Barsoum, T. El-Raghy, Ti_3SiC_2 has negligible thermopower, Nature 407 (2000) 581–582.
[5] M.W. Barsoum, T. El-Raghy, Synthesis and characterization of a remarkable ceramic: Ti_3SiC_2, J. Am. Ceram. Soc. 79 (7) (1996) 1953–1956.
[6] C.F. Hu, Y.C. Zhou, Y.W. Bao, et al., Tribological properties of polycrystalline Ti_3SiC_2 and Al_2O_3-reinforced Ti_3SiC_2 composites, J. Am. Ceram. Soc. 89 (11) (2006) 3456–3461.
[7] J.F. Zhang, L.J. Wang, W. Jiang, et al., Effect of TiC content on the microstructure and properties of Ti_3SiC_2–TiC composites in situ fabricated by spark plasma sintering, Mater. Sci. Eng. A 487 (1–2) (2008) 137–143.
[8] J.F. Zhang, L.J. Wang, W. Jiang, et al., Rapid fabrication of Ti_3SiC_2–SiC nanocomposite using the spark plasma sintering-reactive synthesis (SPS-RS) method, Scripta Mater. 56 (3) (2007) 241–244.
[9] E. Benko, P. Klimczyk, S. Mackiewicz, et al., cBN–Ti_3SiC_2 composites, Diamond Relat. Mater. 13 (3) (2004) 521–525.
[10] W.B. Zhou, B.C. Mei, J.Q. Zhu, Synthesis of Ti_3SiC_2/TiB_2 composite by in-situ hot pressing (HP) method, J. Wuhan Univ. Tech. Mater. Sci. Ed. 23 (6) (2008) 863–865.
[11] S.L. Shi, W. Pan, Toughening of Ti_3SiC_2 with 3Y-TZP addition by spark plasma sintering, Mater. Sci. Eng. A 447 (1–2) (2007) 303–306.
[12] M.W. Barsoum, L.H. Ho-Duc, M. Radovic, et al., Long time oxidation study of Ti_3SiC_2, Ti_3SiC_2/SiC, and Ti_3SiC_2/TiC composites in air, J. Electrochem. Soc. 150 (4) (2003) B166–B175.
[13] S.B. Li, L.F. Cheng, L.T. Zhang, The morphology of oxides and oxidation behavior of Ti_3SiC_2-based composite at high-temperature, Comp. Sci. Technol. 63 (6) (2003) 813–819.
[14] Z.M. Sun, Y.C. Zhou, M.S. Li, High temperature oxidation behavior of Ti_3SiC_2-based material in air, Acta Mater. 49 (20) (2001) 4347–4353.
[15] T. Chen, P.M. Green, J.L. Jordan, et al., Oxidation of Ti_3SiC_2 composites in air, Metall. Mater. Trans. A: Phys. Metall. Mater. Sci. 33 (6) (2002) 1737–1742.
[16] J.F. Zhang, L.J. Wang, W. Jiang, et al., High temperature oxidation behavior and mechanism of Ti_3SiC_2–SiC nanocomposites in air, Comp. Sci. Technol. 68 (2008) 1531–1538.
[17] J. Yang, L.M. Pan, W. Gu, et al., Microstructure and mechanical properties of in-situ synthesized (TiB_2 + TiC)/Ti_3SiC_2 composites, Ceram. Int. 38 (1) (2012) 649–655.
[18] R.A. Young, The Rietveld Method, Oxford University press, 1993.
[19] J.P. Zhang, Y. Sun, G. Yang, Synthesis, characterization and study on vibration spectra of potassium triborate, Spectrosc. Spect. Anal. 27 (7) (2007) 1351–1354.
[20] J.Y. Wang, M. Wang, F. Yuan, Luminescenct spectra and IR spectra of Tb^{3+}-doped zinc borate glasses, Chin. J. Light Scatter. 20 (4) (2008) 353–355.
[21] M.W. Barsoum, T. El-Raghy, Oxidation of Ti_3SiC_2 in air, J. Electrochem. Soc. 144 (7) (1997) 2508–2516.